Research Square

Preprints are preliminary reports that have not undergone peer review.
They should not be considered conclusive, used to inform clinical practice,
or referenced by the media as validated information.

# Spectroscopic, Thermal and Electrical Evaluation of CNT-Modified PVC/PMMA Blends

**Afşar Çelik**

afsarcelik1971@gmail.com

Van Yuzuncu Yil Universitesi Fen Bilimleri Enstitusu https://orcid.org/0000-0002-5824-8338

**Mustafa Hamdi Karagöz**

**Research Article**

**Keywords:** PVC/PMMA blend, carbon nanotube, thermal analysis, electrical conductivity, morphology

**Posted Date:** March 5th, 2026

**DOI:** https://doi.org/10.21203/rs.3.rs-8926644/v1

**License:** This work is licensed under a Creative Commons Attribution 4.0 International License.
Read Full License

**Version of Record:** A version of this preprint was published at Journal of Polymer Research on June 6th, 2026. See the published version at https://doi.org/10.1007/s10965-026-04962-y.

# Spectroscopic, Thermal and Electrical Evaluation of CNT-Modified PVC/PMMA Blends

Afşar Çelik*, Mustafa Hamdi Karagöz

Institute of Science, Van Yüzüncü Yıl University, Van, Turkey

Department of Chemistry, Faculty of Science, Van Yüzüncü Yıl University, Van, Turkey

*Corresponding author: afsarcelik1971@gmail.com

Abstract

This study presents a systematic evaluation of the spectroscopic, thermal, morphological, and electrical behavior of PVC/PMMA blends reinforced with 0.1–1 wt% carbon nanotubes (CNTs) at three different PVC ratios (40%, 50%, and 80%). A total of twelve nanocomposites were fabricated using a solvent-casting method to investigate how blend composition and CNT loading cooperatively influence structure–property relationships. DSC analyses revealed a single glass-transition temperature (Tg ≈ 60–70 °C) for all samples, confirming complete miscibility between PVC and PMMA. XRD patterns demonstrated the preservation of amorphous character across all formulations, while minor fluctuations in crystallinity were observed depending on CNT concentration. TGA measurements indicated typical multi-step thermal degradation behavior, with initial mass losses near 194 °C and main-chain decomposition occurring above 340 °C, showing that CNT addition did not substantially alter overall thermal stability.

SEM micrographs confirmed homogeneous CNT dispersion and revealed composition-dependent morphological arrangements that directly correlated with electrical performance. Electrical conductivity measurements exhibited a clear percolation threshold in the 50:50 blend: PVC50–1 achieved ~$10^{-6}$ S/cm, marking the onset of semiconducting behavior, whereas PVC40 and PVC80 required higher CNT connectivity to reach comparable values. Interfacial energy calculations based on the Owens–Wendt model predicted preferential CNT localization within the PVC phase, supporting the experimentally observed conductivity enhancement in PVC-rich domains and explaining why optimal percolation occurs only when CNT localization and phase continuity coincide.

Overall, the results demonstrate that modulating the PVC/PMMA ratio is an effective strategy for controlling CNT distribution, percolation network formation, and charge-transport properties. The synergistic influence of blend composition and CNT loading provides valuable insight into designing PVC/PMMA/CNT nanocomposites for antistatic, flexible electronic, and low-cost semiconductive applications.

**Keywords:** PVC/PMMA blend; carbon nanotube; thermal analysis; electrical conductivity; morphology.

## Introduction

Polymer blends are physical mixtures of two or more polymers designed to generate new materials with improved or tunable physical properties. As the development of entirely new polymers is often costly and time-consuming, blending has emerged as a practical and economical strategy to achieve tailored performance characteristics. Since the early 2010s, polymer blending has represented a significant portion of the plastics industry due to its capacity to combine the advantageous properties of multiple polymers into a single material **[1,2]**.

Polymer nanocomposites constitute a more advanced class of hybrid materials in which inorganic nanoparticles—typically at least one-dimensionally nanoscale—are uniformly dispersed within a polymer matrix. The incorporation of nanoscale fillers is known to improve mechanical strength, thermal stability, electrical conductivity, optical behavior, and barrier properties **[3]**. Over the past several decades, such nanocomposites have become essential in applications ranging from biomedical devices and membrane technologies to functional textiles, catalysis, electronics, and drug delivery systems **[4,5]**. What makes polymer nanocomposites particularly attractive is the synergistic interaction between the polymer matrix and the nanofillers, which enhances structural, electrical, mechanical, and chemical performance while maintaining low production costs and high processability **[6]**.

Among polymer blends, the PVC/PMMA system has been studied extensively due to its favorable mechanical properties, processability, and morphological compatibility. One of the earliest investigations, conducted by Schurer et al. **[7]**, examined the influence of

PMMA tacticity on its compatibility with PVC. Later, Hong et al. **[8]** investigated the effect of solvent quality on PVC/PMMA miscibility by analyzing Huggins' constant (k′). Their findings indicated that tetrahydrofuran (THF) acts as a strong solvent for PVC (k′ ≈ 0.6) but only a weak solvent for PMMA (k′ ≈ 0.87), highlighting differences in solvation behavior that directly affect blend morphology. Saeed and Khan **[9]** studied PMMA/PVC blends reinforced with functionalized multi-walled carbon nanotubes (F-MWCNTs) and reported that increasing F-MWCNT content led to a gradual decrease in mechanical performance for both α- and β-type blends, emphasizing the sensitivity of mechanical behavior to filler concentration.

Further investigations have demonstrated that PVC/PMMA blends maintain their miscibility even in the presence of different inorganic fillers. El-Gamal and El-Sayed **[10]** reported single glass transition temperatures (82–85 °C) in PbO-doped PVC/PMMA blends, confirming retained miscibility despite nanoparticle incorporation. PbO addition also enhanced thermal stability and increased Young's modulus by 12–18%. Similarly, Mohammed et al. **[11]** demonstrated that MgO doping does not disturb the morphology of PVC/PMMA blends, and free-volume, FTIR, and optical analyses showed that intermolecular interactions between PVC and PMMA remain intact. Collectively, these studies establish that PVC/PMMA blends form a stable single-phase system even after the incorporation of diverse nanofillers.

In designing the present study, PVC compositions of 40%, 50%, and 80% were selected to represent PMMA-rich, compositionally balanced, and PVC-rich regimes, respectively. CNT loadings of 0.1–1 wt% were chosen because this range commonly corresponds to the

region in which electrical percolation phenomena emerge in CNT-reinforced polymer systems. El-Naggar et al. (2023) **[12]** demonstrated that CNT incorporation enhances electrical, dielectric, and optical performance without compromising matrix stability, supporting the hypothesis that CNTs act as structural and functional reinforcement agents in polymer blends.

The electrical behavior of CNT-filled composites can be rationalized using percolation theory. In nanocomposite systems consisting of insulating matrices and conductive fillers, conductivity increases sharply once the filler fraction exceeds a critical value known as the percolation threshold **[13,14]**. This relationship can be expressed mathematically by the power-law equation given in Eq. (1).

$$\sigma = \sigma_0 (P - Pc)^t \qquad (1)$$

Where $\sigma_0$ is a proportionality constant, P is the CNT weight fraction, Pc is the percolation threshold, and t is a critical exponent dependent on filler conductivity, interfacial contact resistance, and network topology **[15,16]**.

Although numerous studies have been conducted on PVC/PMMA blends and CNT-based nanocomposites, most have focused on a narrow range of compositions and filler concentrations. A systematic investigation combining multiple PVC/PMMA ratios with multiple CNT loadings is notably absent from the literature. Therefore, this study aims to address this gap by examining how three different blend compositions (40%, 50%, and 80% PVC) interact with varying CNT contents (0.1–1 wt%) to influence the morphological, thermal, and electrical behavior of the PVC/PMMA system.

The interfacial affinity between CNTs and the polymer phases was evaluated using the Owens–Wendt two-parameter surface-energy model, originally proposed by Owens and Wendt (1969). This model separates the total surface tension of each material into dispersive ($\gamma^D$) and polar ($\gamma^p$) components and computes the CNT–polymer interfacial energy ($\gamma_{12}$) through geometric-mean interactions of these components. Because lower $\gamma_{12}$ values indicate better wetting and stronger interfacial compatibility, the model provides a quantitative basis for determining whether CNTs preferentially interact with PVC or PMMA. The surface-energy values summarized in Table 1 were inserted into this equation to obtain the interaction terms that govern CNT phase preference within the blend. The interfacial energy between CNTs and each polymer phase was calculated using the Owens–Wendt equation, expressed as follows:

$$\gamma_{12} = \gamma_1 + \gamma_2 - 2(\sqrt{(\gamma_1^D \gamma_2^D)} + \sqrt{(\gamma_1^P \gamma_2^P)}) \qquad (2)$$

The preferential localization of carbon nanotubes (CNTs) in multiphase polymer blends is governed by the minimization of interfacial free energy, a thermodynamic principle first adapted to nanofillers by Ajayan and Schadler (2003). In such systems, CNTs selectively migrate toward the polymer phase that provides the lowest CNT–polymer interfacial tension, a behavior consistent with classical wetting theory **[17,18]**.

Table 1. Surface energy components and wetting parameters of CNT (MWCNT), PMMA, and PVC reported in the literature.

| **Material / Interface** | **γ (mN/m)** | **$\gamma^d$ (mN/m)** | **$\gamma^p$ (mN/m)** | **γ_{CNT/A} (mN/m)** | **Notes / Interpretation** | **References** |
|---|---|---|---|---|---|---|
| **CNT (MWCNT)** | 40–45 | 30–35 | 5–10 | – | High surface energy carbonaceous filler | Shen et al., 2009; Coleman et al., 2006 |
| **PMMA** | 39–41 | 34–36 | 4–5 | **4.5–6.0** | CNT–PMMA interfacial tension is low → strong affinity | Owens & Wendt 1969; Wu 1982; Mittal 1993 |
| **PVC** | 33–36 | 28–30 | 3–6 | **8.0–10.0** | CNT–PVC interfacial tension is higher → weak affinity | Van Oss 1988; Wu 1982 |
| **Wetting Coefficient** (W_{PMMA/PVC}) | – | – | – | – | **W ≈ +3.5 to +4.0 → CNT preferentially wets PMMA phase** | Zhang et al., 2015; Sarvi & Sundararaj, 2016 |

Interfacial tensions (γ_{CNT/A}) were calculated using the Owens–Wendt surface energy model, which decomposes polymer and filler surface energies into dispersive and polar components (Owens & Wendt, 1969). The calculated wetting coefficient (W_{PMMA/PVC} ≈ +3.5–4.0) clearly indicates a strong thermodynamic preference of CNTs for the PMMA phase rather than the PVC phase, consistent with previously reported experimental observations **[19,20]**.

The quantitative description of this phenomenon relies on the wetting coefficient, defined as Eq. (3):

$$W = (\gamma_(CNT, PVC) - \gamma_(CNT, PMMA)) / \gamma_(PMMA, PVC) \quad (3)$$

where γ denotes the CNT–polymer interfacial tensions. These interfacial tensions are commonly estimated through the Owens–Wendt surface energy model, which decomposes surface energies into dispersive and polar components (Owens & Wendt, 1969).

The value of the wetting coefficient predicts CNT localization regimes:

$W<-1$: complete wetting of the A phase

$-1<W<+1$: localization at the interface

• $W> +1$: complete wetting of the B phase

This classification, originally introduced by Balazs et al. (2000), has been widely validated for CNT-filled polymer blends **[21,22]**.

Importantly, CNT localization plays a critical role in determining the morphology, double-percolation behavior, and ultimately the electrical conductivity of polymer blends. When CNTs selectively wet a single phase, a continuous conductive network forms at comparatively low filler loadings, whereas interfacial localization enables double-percolation mechanisms, significantly lowering the effective percolation threshold **[20,22,23]**.

Given that PMMA generally exhibits a higher surface energy than SAN or PVC, CNTs are frequently reported to preferentially localize in the PMMA-rich domains **[19]**, a trend consistent with thermodynamic predictions from the wetting coefficient formalism.

Understanding CNT localization is crucial because the phase in which CNTs preferentially reside directly determines the blend morphology, the onset of double percolation, and ultimately the electrical conductivity **[20,22,23]**. For this reason, the wetting coefficient is

introduced here as a predictive tool that links interfacial energetics to the expected CNT distribution and provides a theoretical basis for interpreting the experimental findings presented in the Results section.

While the Owens–Wendt approach and the resulting wettability coefficient (ω) provide a valuable thermodynamic insight into CNT–polymer interactions, they represent a tendency rather than an absolute prediction. These parameters therefore serve as a theoretical guide that complements the experimental observations presented in this study. Although the Owens–Wendt model predicts preferential CNT wetting of PMMA, the actual localization in multiphase blends can also be influenced by solvent–polymer interactions and phase continuity. These complementary mechanisms, and their implications for percolation and electrical behavior, are examined in the Discussion section.

**Material and Methods**

Poly(methyl methacrylate) (PMMA, Mw ≈ 15,000), low-molecular-weight PVC, multi-walled carbon nanotubes (CNTs, 6–13 nm diameter, 2.5–20 μm length, >98% purity), and analytical-grade tetrahydrofuran (THF, >99.9%) were all supplied by Sigma-Aldrich. A Dathan MS-MP8 magnetic stirrer and a Lab Companion ultrasonic cleaner were used to prepare the nanocomposite dispersions.

The preparation method followed Yanmaz **[15]** with appropriate modifications. PVC/PMMA blends were produced at 40:60 and 50:50 and 80:20 weight ratios by dissolving the corresponding amounts of PVC and PMMA in THF. CNTs were introduced at 0.1, 0.5, and 1 wt% relative to the total polymer mass. First, CNTs were dispersed in THF, and this dispersion was added to 30 mL of polymer solution. The resulting mixture

was sonicated for two hours to promote uniform CNT dispersion and subsequently stirred magnetically at 600 rpm for one hour. The homogenized dispersions were cast onto Petri dishes and left to dry at room temperature for 24 hours, yielding free-standing nanocomposite films.

Blend codes were assigned according to PVC content (PVC40, PVC50, PVC80), while nanocomposites were additionally labeled based on CNT concentration (0, 0.1, 0.5, and 1 wt%). Accordingly, samples were coded as PVC40-0, PVC40-0.1, PVC40-0.5, PVC40-1, and similarly for the 50% and 80% blends.

Morphological analyses were performed using a Sigma 300 FE-SEM. Structural characterization was carried out using a Rigaku Ultima IV X-ray diffractometer. Thermal stability was evaluated using a Hitachi STA 7300 TGA/DTA instrument, while glass-transition behavior was examined via DSC using a PerkinElmer Diamond calorimeter. Since the glass-transition temperatures of pure PVC and PMMA lie below 100 °C, DSC measurements were limited to this temperature range. Although DSC scans covered a wider temperature range, only the region containing the glass-transition event was evaluated and presented, as the purpose of this study was limited to determining Tg rather than identifying additional endothermic transitions at higher temperatures." Electrical conductivity measurements were performed with a Keithley 6517A Electrometer.

**Experimental**

Macroscopic inspection showed increasing brittleness in PVC40 samples as CNT loading decreased (Fig. 1).

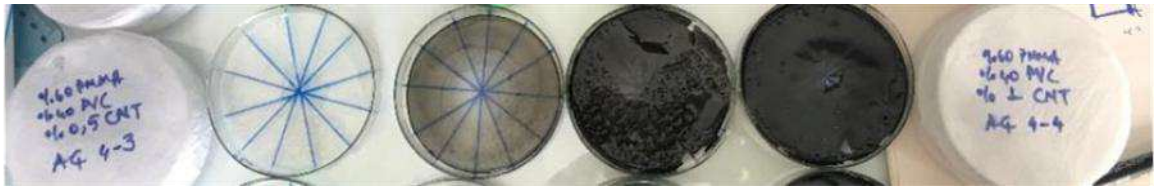
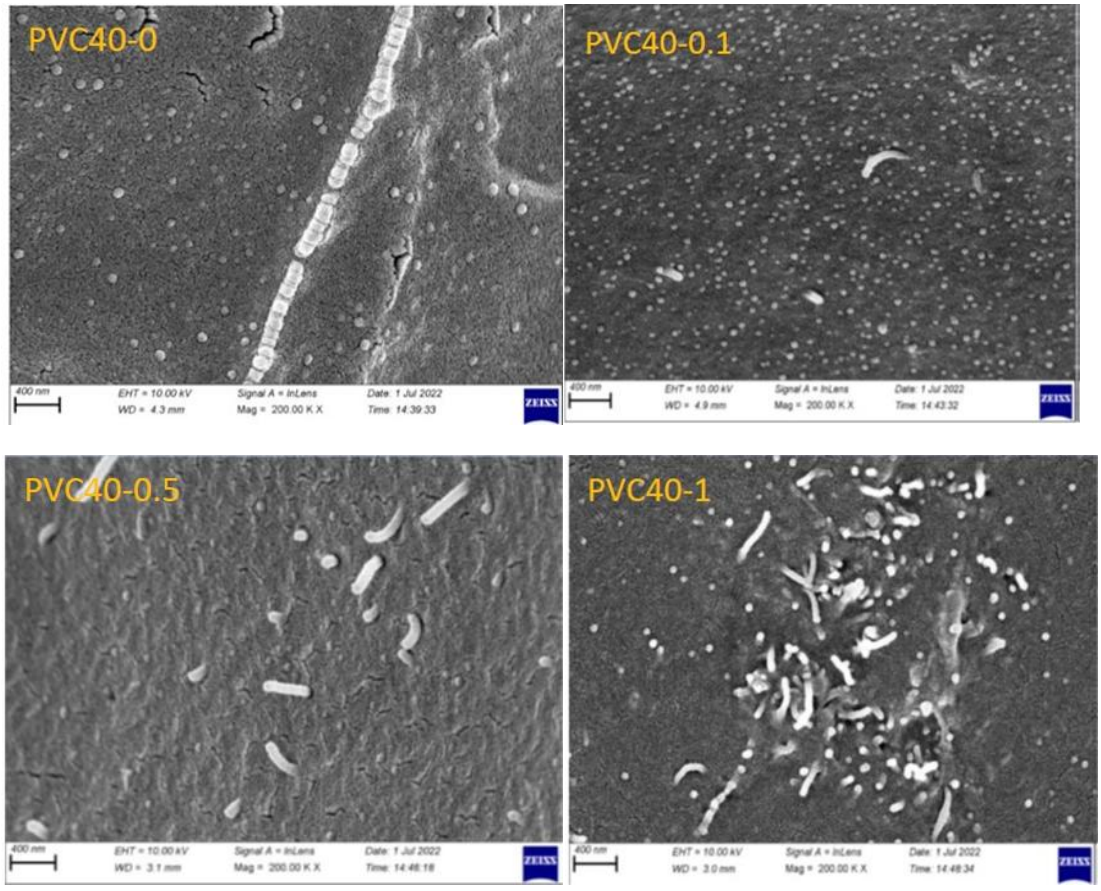
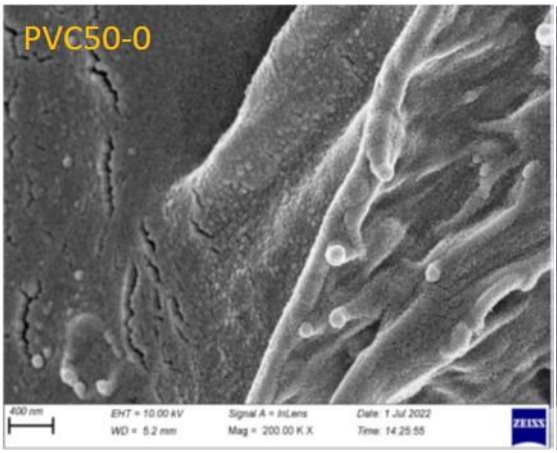
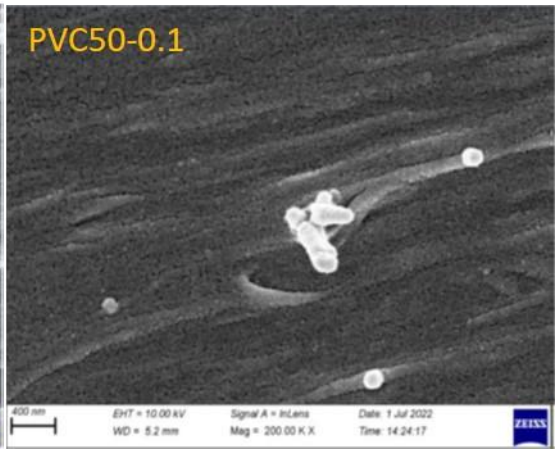


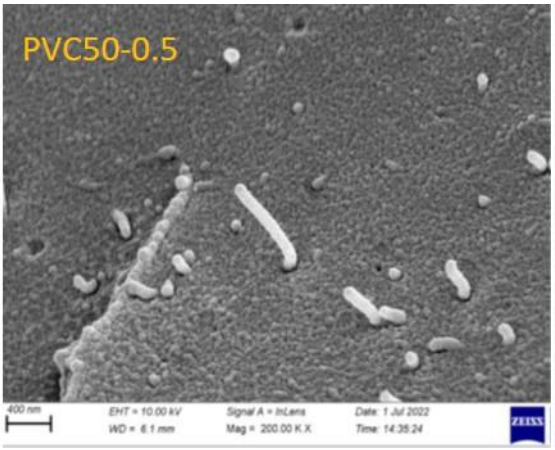
Figure 1. Fragility in PVC40 (0-1) Series

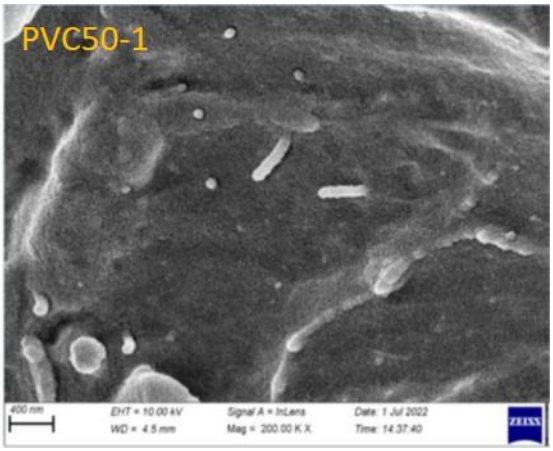
SEM micrographs revealed PMMA-rich domains in PVC40 and more continuous PVC phases in PVC50 (Fig. 2).

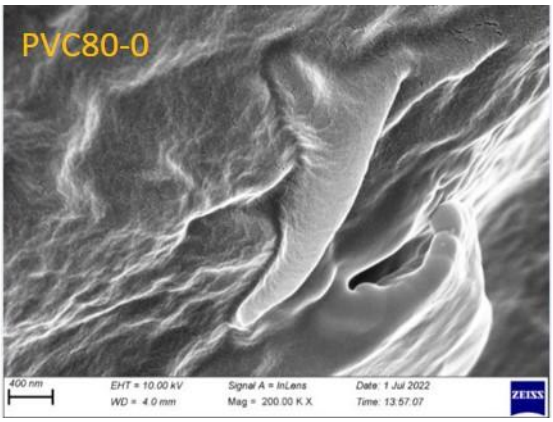


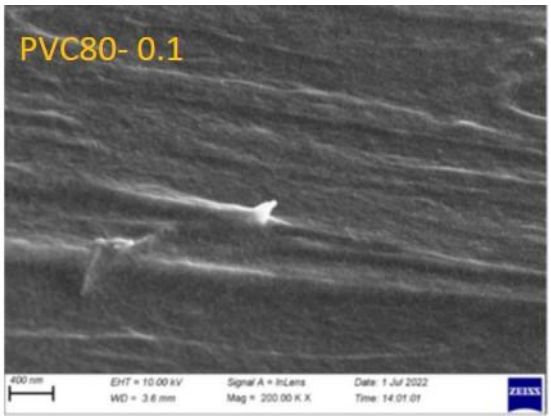

PVC50-0
400 nm
EHT = 10.00 kV
WD = 5.2 mm
Signal A = InLens
Mag = 200.00 K X
Date: 1 Jul 2022
Time: 14:25:55
ZEISS


PVC50-0.1
400 nm
EHT = 10.00 kV
WD = 5.2 mm
Signal A = InLens
Mag = 200.00 K X
Date: 1 Jul 2022
Time: 14:24:17
ZEISS


PVC50-0.5
400 nm
EHT = 10.00 kV
WD = 6.1 mm
Signal A = InLens
Mag = 200.00 K X
Date: 1 Jul 2022
Time: 14:35:24
ZEISS


PVC50-1
400 nm
EHT = 10.00 kV
WD = 4.5 mm
Signal A = InLens
Mag = 200.00 K X
Date: 1 Jul 2022
Time: 14:37:40
ZEISS


PVC80-0
400 nm
EHT = 10.00 kV
WD = 4.0 mm
Signal A = InLens
Mag = 200.00 K X
Date: 1 Jul 2022
Time: 13:57:07
ZEISS


PVC80- 0.1
400 nm
EHT = 10.00 kV
WD = 3.6 mm
Signal A = InLens
Mag = 200.00 K X
Date: 1 Jul 2022
Time: 14:01:01
ZEISS

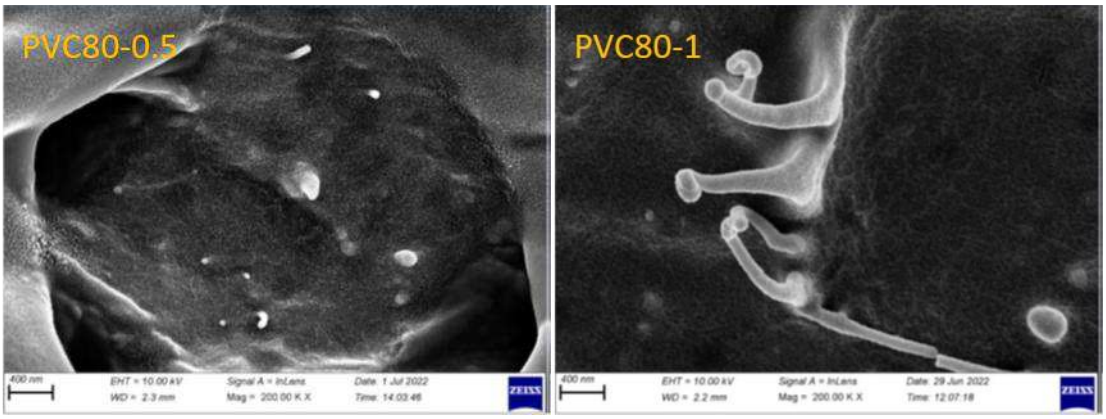



Figure 2. PVC40,PVC50 and PVC80 (0-1) SEM images at 200,000× magnification

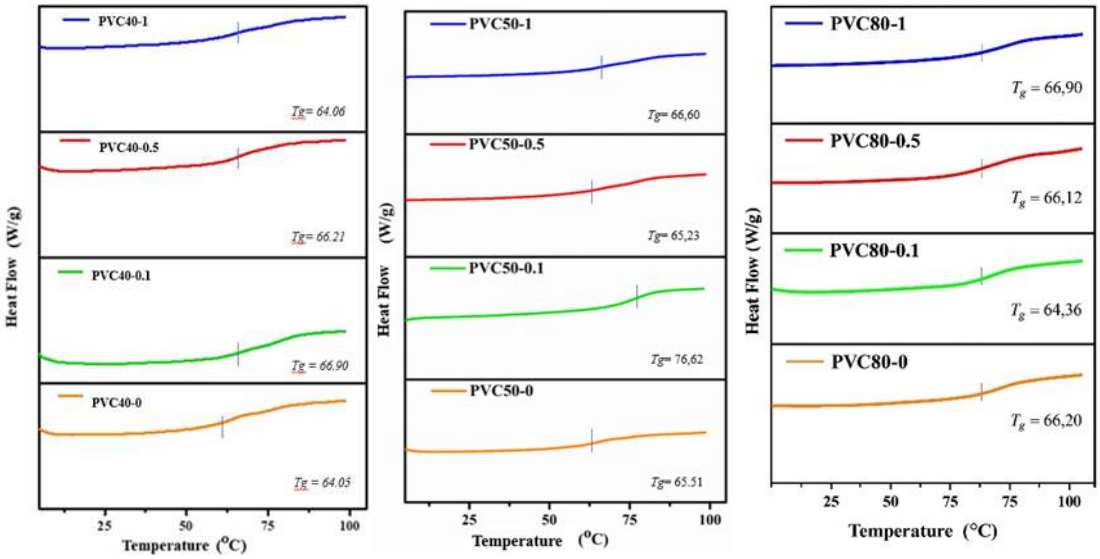



Figure 3. PVC40-50- (0-1) Series DSC curves

Table 2. PVC40-50(0-1) Series Tg Values

| Sample Code | Tg (°C) |
|---|---|
| **PVC40-0** | 64.05 |
| **PVC40-0.1** | 66.90 |
| **PVC40-0.5** | 66.21 |
| **PVC40-1** | 64.06 |
| **PVC50-0** | 65.51 |
| **PVC50-0.1** | 76.62 |
| **PVC50-0.5** | 65.23 |
| **PVC50-1** | 66.60 |
| **PVC80-0** | 66.20 |
| **PVC80-0.1** | 64.36 |
| **PVC80-0,5** | 66.12 |
| **PVC80-1** | 66.90 |

All blends exhibited a single Tg, confirming miscibility across all CNT loadings (Fig. 3; Table 2)

Among all samples, PVC50–0.1 exhibited an unusually high Tg compared to the rest of the series. The pronounced **Tg increase observed specifically in the PVC50–0.1 sample** can be explained by the combined effect of several interconnected mechanisms activated at low CNT loading. First, preferential wetting of PMMA by CNTs restricts local chain mobility within PMMA-rich domains, which can produce a notable upward shift in Tg when dispersion is efficient [23]. Second, CNTs tend to accumulate at phase boundaries in heterogeneous PVC/PMMA blends, a phenomenon known to induce **interfacial rigidification**, thereby elevating the effective glass transition temperature **[24]**. Third, at low CNT content, selective localization within the PMMA phase may promote the formation of a partial micro-network, reducing free volume and strengthening chain–CNT interactions **[25]**. Thus, the anomalous Tg value of the PVC50–0.1 sample is best interpreted as the **combined result of enhanced dispersion, interfacial stiffening, and selective localization at low CNT loading**, rather than a trend representative of the entire PVC50 series.

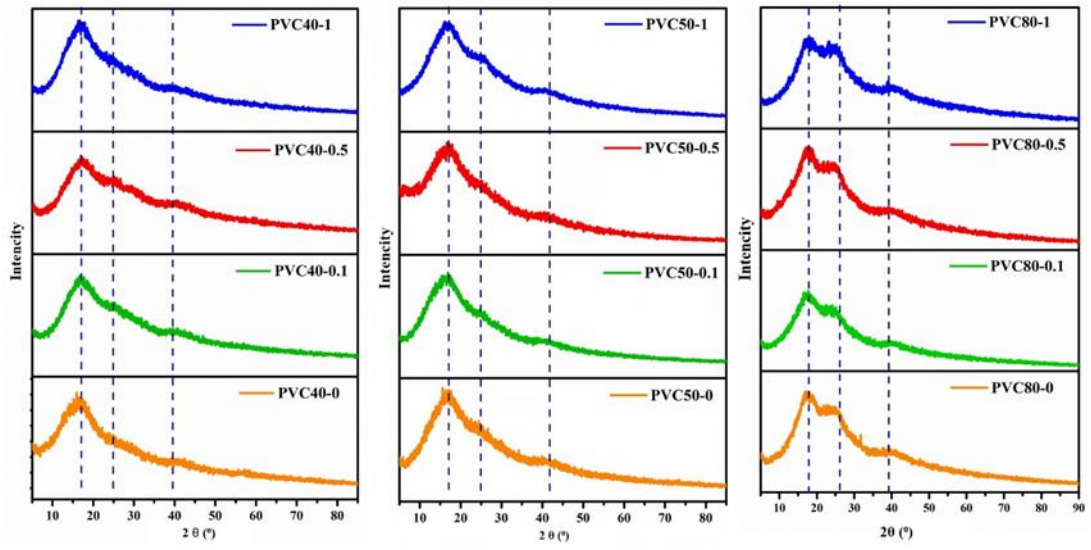


Figure 4. PVC40,50,80 (0-1) Series XRD curves.

XRD patterns verified the amorphous nature of all compositions (Fig. 4; Table3).

Table 3. PVC40,50,80 (0-1) Series angles and crystallinities

| Sample Code | 2 θ | Crystallinity % | Sample Code | 2 θ | Crystallinity % | Sample Code | 2 θ | Crystallinity % |
|---|---|---|---|---|---|---|---|---|
| **PVC40-0** | 16.18 | 15.69 | **PVC50-0** | 17.04 | 15.47 | **PVC80-0** | 17.74 | 15.71 |
| | 23.54 | | | 24.44 | | | 23.42 | |
| | 39.74 | | | 39.88 | | | 39.34 | |
| **PVC40-0.1** | 16.68 | 14.97 | **PVC50-0.1** | 16.92 | 14.1 | **PVC80-0.1** | 17.28 | 15.9 |
| | 23.56 | | | 24.68 | | | 23.74 | |
| | 38.74 | | | 38.98 | | | 39.76 | |
| **PVC40-0.5** | 17 | 15.11 | **PVC50-0.5** | 16.68 | 14.17 | **PVC80-0.5** | 17.94 | 15.86 |
| | 25.18 | | | 23.96 | | | 22.94 | |
| | 40.44 | | | 41.58 | | | 39.86 | |
| **PVC40-1** | 16.78 | 15.7 | **PVC50-1** | 17.18 | 15.38 | **PVC80-1** | 17.52 | 14.61 |
| | 23.28 | | | 23.22 | | | 23.3 | |
| | 38.92 | | | 40.34 | | | 39.14 | |

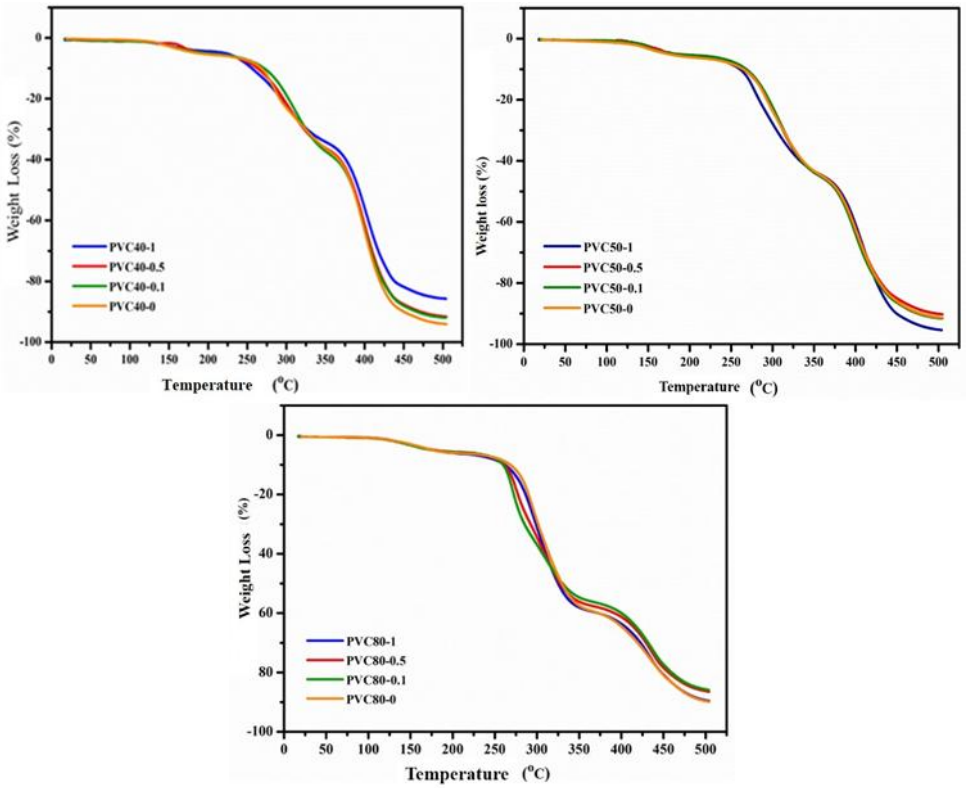



Figure 5. PVC40-50 (0-1) Series TGA curves

Thermal degradation proceeded through three typical steps, with the main-chain decomposition above 340 °C (Fig. 5; Table 4).

Table 4 PVC40,50,80 (0-1) Series TGA values

| Sample Code | T1 (°C) | Weight Loss % | T2 (°C) | Weight Loss % | T3 (°C) | Weight Loss % | Tf (°C) | Maximum Weight Loss % |
|---|---|---|---|---|---|---|---|---|
| **PVC40-0** | 194.11 | 5.26 | 349.42 | 36.16 | 442.95 | 88.92 | 473.70 | 92.61 |
| **PVC40-0.1** | 193.39 | 4.86 | 348.72 | 36.98 | 442.19 | 86.78 | 473.01 | 90.61 |
| **PVC40-0.5** | 194.09 | 5.02 | 349.43 | 36.07 | 442.28 | 80.80 | 473.62 | 90.15 |
| **PVC40-1** | 193.42 | 4.26 | 348.60 | 33.99 | 442.29 | 87.97 | 473.01 | 84.32 |
| **PVC50-0** | 194.73 | 5.91 | 349.98 | 43.29 | 443.32 | 84.53 | 474.04 | 89.55 |
| **PVC50-0.1** | 193.67 | 5.22 | 349.96 | 43.79 | 442.88 | 85.01 | 473.68 | 89.83 |
| **PVC50-0.5** | 194.56 | 5.56 | 349.71 | 43.36 | 443.03 | 83.68 | 473.93 | 88.33 |
| **PVC50-1** | 193.54 | 5.66 | 348.81 | 43.19 | 442.29 | 87.97 | 473.07 | 93.43 |
| **PVC80-0** | 194.22 | 5.84 | 349.42 | 57.40 | 442.73 | 78.45 | 473.45 | 86.49 |
| **PVC80-0.1** | 193.24 | 5.60 | 348.49 | 54.48 | 441.96 | 74.42 | 472.77 | 82.85 |
| **PVC80-0.5** | 193.73 | 5.47 | 349.01 | 56.00 | 442.45 | 75.83 | 473.27 | 83.55 |
| **PVC80-1** | 193.81 | 5.87 | 348.10 | 57.92 | 442.45 | 78.27 | 473.23 | 86.33 |

Table 5. PVC40,50,80 (0-1) Series Ea Values

| Sample Code | Ea 1 (kj/mol) | Ea 2 (kj/mol) | Ea 3 (kj/mol) |
|---|---|---|---|
| PVC40-0 | 132.80 | 119.81 | 106.55 |
| PVC40-0.1 | 133.26 | 119.30 | 106.69 |
| PVC40-0.5 | 132.97 | 119.55 | 106.54 |
| PVC40-1 | 133.77 | 119.44 | 106.66 |
| Average | 133.20 | 119.52 | 106.60 |
| PVC50-0 | 131.54 | 117.41 | 107.48 |
| PVC50-0.1 | 132.60 | 117.29 | 107.34 |
| PVC50-0.5 | 131.94 | 117.23 | 107.31 |
| PVC50-1 | 132.24 | 117.91 | 107.59 |
| Average | 132.09 | 117.46 | 107.44 |
| PVC80-0 | 131.33 | 113.25 | 109.09 |
| PVC80-0.1 | 131.27 | 113.36 | 109.38 |
| PVC80-0.5 | 131.58 | 113.10 | 109.07 |
| PVC80-1 | 131.26 | 113.06 | 109.08 |
| Average | 131.36 | 113.19 | 109.16 |

TGA weight loss percentages and temperatures are given in Tab. 4. The activation energies are obtained within single heat rate, calculated from Coats Redfern Equation Eq. (4) and presented in Tab. 5.

$$\log\left(\frac{-\ln(1-\alpha)}{T^2}\right) = \log\left(\frac{AR}{\beta E_a}\right) - \frac{E_a}{2.303RT} \quad \text{Equation (4)}$$

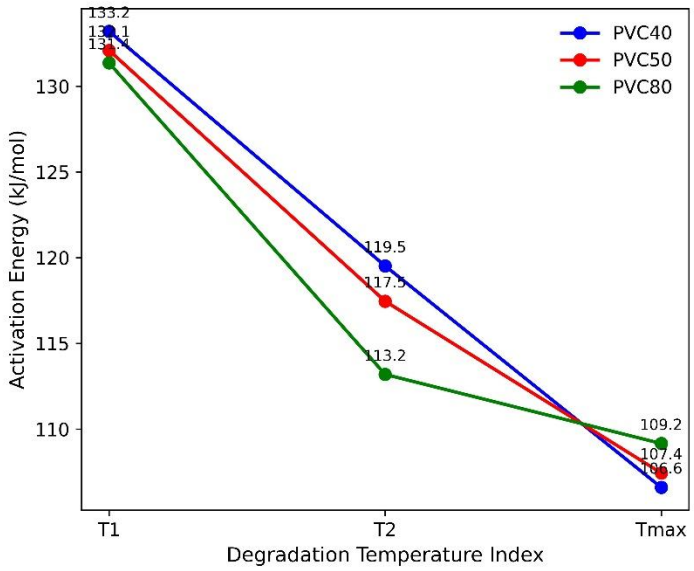



Figure 6. PVC40-50-80 (0-1) Series average activation energy values

Table 6. PVC 40-50-80 Series Electrical Conductivities

| CNT % | PVC40 σ (S/cm) | CNT (%) | PVC50 σ (S/cm | CNT (%) | PVC80 σ (S/cm) |
|---|---|---|---|---|---|
| 0 | 7.69*10-16 | 0 | 1.58*10-17 | 0 | 2.94*10-15 |
| 0.1 | 1.50*10-15 | 0.1 | 1.89*10-16 | 0.1 | 5.05*10-15 |
| 0.5 | 4.5*10-13 | 0.5 | 6.21*10-7 | 0.5 | 2.98*10-7 |
| 1 | 1.27*10-7 | 1 | 4.97*10-6 | 1 | 6.94*10-8 |

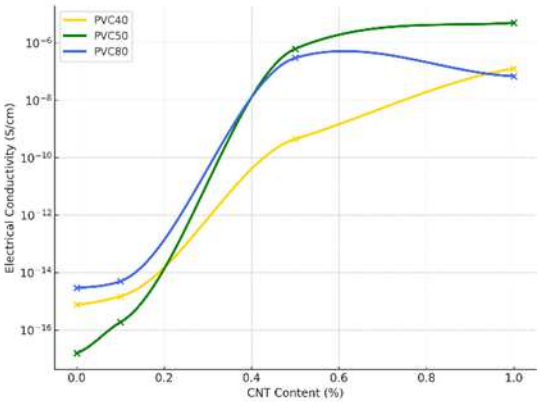



Figure 7. PVC40-50-80 (0-1) Series electrical conductivity curve

A clear percolation threshold appeared in the PVC50 blend at 1 wt% CNT (Fig. 6; Table 6).

**Discussion**

The first indication of structural fragility appeared in the macroscopic images of the PVC40 series (Fig. 1), where pronounced surface cracking was observed, especially in the CNT-free and low-CNT samples. Although these cracks were visually apparent at the macro scale, the corresponding SEM micrographs (Fig. 2) did not display fracture-like features or microcrack propagation patterns. This suggests that the brittleness is not governed by localized microscale defects but rather by broader phase-distribution effects within the matrix. SEM analysis revealed pronounced PMMA-rich regions in PVC40 samples, indicating a reduction in matrix continuity and, consequently, mechanical integrity. Thus, the interpretation of fragility in this series is grounded first in macroscopic visual evidence and then corroborated by SEM-based morphological assessment, which clarifies the structural origin of the observed behavior.

While PMMA-rich microdomains contribute to the increased brittleness in PVC40 samples, CNT incorporation produced a slight but consistent mitigation of this effect. This improvement likely arises from interfacial reinforcement through CNT–polymer interactions, consistent with earlier studies reporting enhanced structural cohesion in CNT-filled polymer systems **[12,13,17,19]**. In the PVC40 series, the clear presence of PMMA-rich zones suggests that dipole–dipole interactions between adjacent PVC chains—particularly Cl–Cl associations—are partially disrupted by PMMA molecules **[15,23]**. Such behavior was not evident in PVC50 samples, underscoring the well-established notion that optimum miscibility and mechanical balance in PVC/PMMA blends occur near the 50:50 composition. Furthermore, SEM results confirmed that CNTs were adequately

dispersed throughout the blends, supporting the mechanical and electrical enhancement mechanisms discussed below.

XRD analyses (Fig. 4; Table 2) demonstrated that all samples preserved their amorphous nature, consistent with prior findings **[16,17,24,25]**. A slight decrease in crystallinity was observed at 0.1 and 0.5 wt% CNT loadings in the PVC40 and PVC50 blends, followed by partial recovery at 1 wt% CNT. Because the CNTs employed in this study were non-functionalized, their interaction with the polymer matrix is expected to rely on non-covalent forces—electrostatic attraction, van der Waals interactions, and micro-mechanical interlocking—rather than chemical bonding **[19,26]**. Similar reductions in crystallinity with nanofiller incorporation have been reported by Althobiti et al. **[23,27]** and in PVC/PMMA/$TiO_2$ nanocomposite systems **[24,28]**.

Thermal degradation proceeded through three stages in all formulations (Fig. 5; Tab. 4). The first mass-loss event concluded near 194 °C, followed by a characteristic dehydrochlorination step beginning around 220 °C, consistent with typical PVC-containing systems **[25,26,29,30]**. Despite the inherent mechanical fragility of CNT-modified structures, DSC measurements revealed a single glass-transition temperature for all blends and all CNT loadings (Fig. 3; Tab. 2). The presence of a single Tg in every case strongly supports the miscibility of PVC and PMMA, confirming their single-phase behavior in agreement with established criteria **[27,31]**. Moreover, the Tg values exhibited no systematic dependence on CNT content, indicating that CNT incorporation does not disrupt the intermolecular interactions governing PVC/PMMA compatibility.

The activation energies of the three degradation stages, calculated using the Coats–Redfern method (Tab. 5), remained within narrow ranges for all CNT loadings, indicating that the incorporation of 0.1–1 wt% CNT does not significantly alter the intrinsic degradation kinetics of the PVC/PMMA matrix. In contrast, the second degradation stage (dehydrochlorination) exhibited a clear dependence on blend composition, with $Ea_2$ decreasing as PVC content increased. This behavior suggests that degradation kinetics are governed primarily by phase composition rather than nanotube-induced chemical stabilization. Activation energies are represented by average activation energies and they are presented in Fig. 6 and Tab.5.

The absence of a significant kinetic change despite enhanced electrical conductivity confirms that conductivity improvement originates from morphology-driven percolation network formation rather than from thermally induced chemical effects.

Electrical conductivity exhibited a distinctly composition-dependent trend (Fig.7, Tab. 6.). In PVC40, the conductivity reached $1.2 \times 10^{-7}$ S/cm at 1 wt% CNT, whereas in PVC50 samples a pronounced percolation threshold became evident. No substantial increase in conductivity was observed until CNT loading reached 1 wt%. This behavior suggests that solvent–polymer interactions may regulate CNT network formation, consistent with the interpretation proposed by Sah and Gupta **[29,32]**. At the 50:50 composition, PVC dominates the matrix sufficiently to allow chain rearrangement and facilitate CNT bridging. As a result, the PVC50–1 sample reached the lower boundary of the semiconducting regime (~$10^{-6}$ S/cm) with only 1 wt% CNT (Fig. 7; Tab. 6). These observations align with Zare et al. **[30,33]**, who reported that PVC/MWCNT

nanocomposites possess one of the highest interfacial conductivity parameters (Lc) among polymer–CNT systems.

Morphological analysis provides direct support for these electrical findings. SEM micrographs of the PVC50–1 sample (Fig. 2) revealed that CNTs were distributed across both polymer phases—partially located within PMMA regions and more prominently dispersed within PVC-rich domains—allowing CNTs to act as interphase bridges. This dual-phase distribution promotes both mechanical continuity and electron transport. In the PVC80–1 sample, however, CNTs tended to localize deeper within PVC-rich regions, occasionally forming small aggregates. While this arrangement maintains structural cohesion, it results in fewer accessible conductive pathways compared to PVC50–1, where CNTs form extended microscale networks. This difference in network architecture directly explains the pronounced conductivity jump observed at 1 wt% CNT in the PVC50 blend.

The superior electrical performance of the PVC50 composition can be further understood through polymer–solvent interaction theory. Previous studies **[32,34]** have shown that THF is a strong solvent for PVC but a relatively weak solvent for PMMA, preferentially swelling PVC domains. This enhances free volume in PVC-rich phases and promotes CNT dispersion, thereby increasing CNT–CNT contact probability. Hong et al. **[29]** reported that the low Huggins interaction parameter for PVC ($k' = 0.6$) facilitates polymer–solvent affinity, enabling PVC chains to unfold more effectively in solution. Consequently, the formation of a conductive CNT network becomes thermodynamically favorable in PVC-dominant compositions. Similar conclusions have been drawn in recent studies **[35,36]**, which demonstrated that THF-mediated swelling improves CNT–matrix coupling and

enhances charge-transport pathways. These insights collectively explain why the 50:50 PVC/PMMA blend presents the most efficient matrix environment for CNT percolation.

These results are consistent with previous reports on CNT-loaded PVC systems and highlight the dominant role of morphology–percolation relationships in determining the structural, thermal, and electrical performance of PVC/PMMA/CNT nanocomposites.

The preferential localization of CNTs in the PVC phase provides a direct explanation for the percolation behavior and electrical conductivity trends observed in this study. As described by the wetting-coefficient expression (Eq. (3)), CNTs migrate toward the polymer phase that minimizes the CNT–polymer interfacial energy, and this interpretation is consistent with the interfacial energy hierarchy summarized in Table 1 **[17,18]**. The markedly higher conductivity of the PVC50–1 sample (Fig. 7; Tab. 6) compared with PVC40 and PVC80 confirms that percolation is optimized only when CNT localization and phase continuity occur simultaneously. THF-induced swelling and enhanced chain mobility in PVC-rich domains further facilitate CNT–CNT contact formation, thereby promoting the development of extended conductive pathways **[29,20]**. Similar behavior has been reported in CNT-reinforced PVC systems, where selective CNT wetting and phase dominance govern charge-transport efficiency **[19,23]**. Altogether, these findings demonstrate that the electrical response of the blends is not solely a function of CNT loading but a direct consequence of thermodynamically driven CNT localization, which dictates network architecture and ultimately determines electron transport across the composite.

## Conclusion

In this study, the combined effects of blend composition and CNT loading on the spectroscopic, thermal, morphological, and electrical behavior of PVC/PMMA nanocomposites were systematically evaluated. DSC measurements consistently revealed a single glass-transition temperature across all formulations, confirming the complete miscibility of PVC and PMMA even in the presence of CNTs. XRD and TGA analyses further demonstrated that CNT incorporation did not alter the amorphous character or the overall thermal stability of the blends. SEM observations indicated that CNTs were well dispersed within the polymer matrix, forming microstructural arrangements that support the observed electrical response.

The electrical behavior was strongly composition-dependent, with the PVC50 blend exhibiting the most pronounced increase in conductivity at 1 wt% CNT. This enhancement can be attributed to the formation of an optimized percolation network, which emerges only when phase continuity and CNT localization act cooperatively. Although the Owens–Wendt model predicts preferential CNT wetting of PMMA, the actual localization observed in this study is dominated by phase continuity and solvent–polymer interactions. In the PVC50 blend, these factors collectively promote CNT alignment within PVC-rich pathways, facilitating continuous CNT–CNT contact formation and enabling an efficient percolation network. As a result, the PVC50–1 sample exhibited the highest conductivity among all formulations, reaching the lower semiconducting regime and confirming that optimal electrical performance emerges only when CNT localization and phase continuity act cooperatively.

Beyond the fundamental structure–property correlations established in this study, the observed combination of controlled percolation behavior, preserved thermal stability, and tunable electrical conductivity suggests potential applicability of the PVC/PMMA/CNT system in lightweight antistatic coatings, low-voltage flexible electronic components, and cost-effective semiconductive films. In particular, the clear percolation threshold observed in the PVC50 composition indicates that conductivity can be precisely tailored through compositional control rather than excessive filler loading. Such morphology-driven conductivity optimization has been reported as a key design strategy in recent polymer/CNT systems developed for printed electronics and smart packaging applications [37,38].

Overall, these findings demonstrate that tuning the PVC/PMMA ratio is an effective strategy for controlling CNT localization, percolation, and charge-transport pathways. The strong correlation between phase morphology and electrical performance highlights the potential of PVC/PMMA/CNT nanocomposites for applications in antistatic coatings, flexible electronic components, and low-cost semiconductive polymer systems.

.

**Acknowledgments**:

This study was supported by the Yüzüncü Yıl University Scientific Research Projects Coordination Unit under Project No. FDK-2020-8776.

**Artificial Intelligence (AI) Usage Statement**

The authors declare that no generative artificial intelligence (AI) tools were used in the design of the study, data collection, data analysis, interpretation of results, or in the development of scientific conclusions presented in this manuscript.

AI-based language tools (ChatGPT) were used solely for linguistic editing, clarity improvement, structural refinement of text, and formatting support.

All scientific content, experimental design, numerical calculations, interpretations, and conclusions were conceived, validated, and approved entirely by the authors. The authors take full responsibility for the integrity, accuracy, and originality of the work.

**Author contributions:**

There are contributions of authors in this article that derived from PhD as below:

Asc. Prof. Mustafa Hamdi Karagöz was contibuted to Conceptial, supervision and advisement. PhD. Afşar Çelik was contributed to Methodology, experimental design, analyses, carrying out measurements, manuscript composition.

Conflicts of interest or competing interests:

The authors declare that there is no conflict of interest or competing interest in this article.

Data and code availability

Data will be made available on request.

Ethical approval:

There is no ethical approval needed for this article

**References**

**[1]** Scobbo JJ, Goettler LA (2003) *Polymer blends handbook*. In: Utracki LA (ed) Kluwer Academic Publishers, Dordrecht.

**[2]** Thomas S, Grohens Y, Jyotishkumar P (2015) *Characterization of polymer blends: miscibility, morphology, and interfaces*. Wiley-VCH, Weinheim.

**[3]** Masoud EM, Liu L, Peng B (2020) Synthesis, characterization, and applications of polymer nanocomposites. *J Nanomater*. DOI:10.1155/2020/5439136

**[4]** İçli S (2006) Polimerik kompozitler: geleceğin teknolojileri. *Polimerik Kompozitler Sempozyumu*, İzmir.

**[5]** Luan J, Wang S, Hu Z, Zhang L (2012) Synthesis techniques, properties and applications of polymer nanocomposites. *Curr Org Synth*.

**[6]** Shameem MM, Sasikanth SM, Annamalai R, Raman RG (2021) A brief review on polymer nanocomposites. *Mater Today Proc*.

**[7]** Schurer JW, de Boer A, Challa G (1975) Influence of PMMA tacticity on compatibility with PVC. *Polymer*.

**[8]** Hong PD, Huang HT, Chou CM (2000) Solvent effect on PVC/PMMA miscibility via viscosity. *Polym Int*.

**[9]** Saeed K, Khan N (2015) Properties of MWCNT-filled PMMA/PVC blends. *J Chem Soc Pak*.

**[10]** El-Gamal S, El-Sayed M (2020) PbO/PVC/PMMA nanocomposites. *Polymer*.

**[11]** Mohammed MI, Ashry A, Ismail AM, Ibrahim MM, Abdel-Hady EE, Awad S (2025) Multifunctional PVC/PMMA/MgO nanocomposites. *Polym Adv Technol*.

**[12]** El-Naggar AM, Alsaggaf A, Heiba ZK, Kamal AM, Aldhafiri AM, Mohamed MB (2023) Impact of MWCNTs on PVA/PANi blends. *J Taibah Univ Sci* 17:1–xx.

**[13]** Ponnamma D, Ninan N, Thomas S (2018) *Applications of nanomaterials*. Woodhead Publishing, Cambridge.

**[14]** Fogel M, Parlevliet P, Geistbeck M et al (2015) MWCNT/epoxy matrices: thermal and electrical analysis. *Compos Sci Technol*.

**[15]** Yanmaz E (2018) *Vinil grubu içeren polimer/modifiye CNT nanokompozitleri*. Dissertation, University of ……

**[16]** Owens DK, Wendt RC (1969) Estimation of the surface free energy of polymers. *J Appl Polym Sci* 13:1741–1747. https://doi.org/10.1002/app.1969.070130815

**[17]** Zhang Q, Chen D, Zhao Y (2015) Selective localization of CNTs in polymer blends. *Compos Sci Technol* 114:1–8. https://doi.org/10.1016/j.compscitech.2015.03.021

**[18]** Sarvi A, Sundararaj U (2016) Morphology and electrical properties of polymer/CNT nanocomposites. *Polymer* 97:1–10. https://doi.org/10.1016/j.polymer.2016.05.040

**[19]** Ajayan PM, Schadler LS, Braun PV (2003) *Nanocomposite science and technology*. Wiley-VCH, Weinheim.

**[20]** Omonov TS, Sundararaj U (2010) CNT migration in polymer blends. *Macromol Mater Eng* 295:698–708. https://doi.org/10.1002/mame.201000087

**[21]** Shen L, Phang IY, Liu T, Zeng K, Chen L (2009) Mechanical properties of CNT–polymer composites. *Mater Sci Eng A* 483–484:105–110. https://doi.org/10.1016/j.msea.2006.09.162

**[22]** Coleman JN, Khan U, Gun'ko YK (2006) Mechanical reinforcement of polymers using CNTs. *Adv Mater* 18:689–706. https://doi.org/10.1002/adma.200501851

**[23]** Mittal KL (1993) *Contact angle, wettability, and adhesion*. VSP, Utrecht.

**[24]** van Oss CJ, Good RJ, Chaudhury MK (1988) Additive and nonadditive surface tension components. *Langmuir* 4:884–891. https://doi.org/10.1021/la00082a018

**[25]** Balazs AC, Singh C, Zhulina E (2000) Modeling polymer–CNT interactions. *Macromolecules* 33:8370–8381. https://doi.org/10.1021/ma000683j

**[26]** Sumfleth J, Adroher XC, Schulte K (2011) Hybrid polymer nanocomposites. *Compos Sci Technol* 71:344–350. https://doi.org/10.1016/j.compscitech.2010.11.018

**[27]** Masarra N, Khelifi A, Mecheri B (2022) Double percolation in polymer blends. *J Appl Polym Sci* 139:e51703. https://doi.org/10.1002/app.51703

**[28]** Chakrabarti R, Das M, Chakraborty D (2004) PVC/PMMA blends. *J Appl Polym Sci*.

**[29]** Dixit M et al (2009) Miscibility and mechanical properties of PMMA/PVC blends. *J Optoelectron Adv Mater*.

**[30]** Sangawar VSA, Moharil AN (2012) Electrical, thermal and optical behavior of PPy-filled PVC/PMMA films. *Chem Sci Trans*.

**[31]** Al-Muntaser A et al (2023) $TiO_2$-enhanced PVC/PMMA nanocomposites. *Polym Eng Sci*.

**[32]** Vouvoudi EC, Rousi AT, Achilias DS (2023) Pyrolysis behavior of polymer blends. *Sustain Chem Pharm*.

**[33]** Ferriol M et al (2003) Thermal degradation of PMMA. *Polym Degrad Stable*

**[34]** Swain SK, Jena I (2010) Polymer/CNT nanocomposites. *Asian J Chem*.

**[35]** Althobiti R et al (2024) Hybrid $TiO_2$/GNP filler in PVC/PMMA blends. *Ceram Int*.

**[36]** Sah GK, Gupta AK (2013) PVC/PMMA miscibility in THF. *Nanosyst Phys Chem Math*.

**[37]** Fenta, E. W., & Mebratie, B. A. (2024). Advancements in carbon nanotube-polymer composites: Enhancing properties and applications through advanced manufacturing techniques. *Heliyon*, *10*(16).

**[38]** Crank, B., Fricker, B., Hubbard, A., Hitawala, H., Muna, F. I., Okunlola, O. S., ... & Schulz, M. (2025). Electromagnetic radiation shielding using carbon nanotube and nanoparticle composites. *Applied Sciences*, *15*(15), 8696.